PCCP

Accepted Manuscript

ROYAL SOCIETY OF CHEMISTRY

www.rsc.org/pccp

Journal Name

RSCPublishing

ARTICLE

Atomically Mixed Fe-Group Nanoalloys: Catalyst Design for the Selective Electrooxidation of Ethylene Glycol to Oxalic Acid

Cite this: DOI: 10.1039/x0xx00000x

Received 00th January 2012,
Accepted 00th January 2012

DOI: 10.1039/x0xx00000x

www.rsc.org/

Takeshi Matsumoto,[a,b] Masaaki Sadakiyo,[a,b] Mei lee Ooi,[a,b] Tomokazu Yamamoto,[b,c] Syo Matsumura,[b,c] Kenichi Kato,[b,d] Tatsuya Takeguchi,[b,e] Nobuki Ozawa,[b,f] Momoji Kubo[f] and Miho Yamauchi[a,b,*]

We demonstrate electric power generation via the electrooxidation of ethylene glycol (EG) on a series of Fe-group nanoalloy (NA) catalysts in alkaline media. A series of Fe-group binary NA catalysts supported on carbon (**FeCo**/C, **FeNi**/C, and **CoNi**/C) and monometallic analogues (**Fe**/C, **Co**/C, and **Ni**/C) were synthesized. Catalytic activities and product distributions on the prepared Fe-group NA catalysts in the EG electrooxidation were investigated by cyclic voltammetry and chronoamperometry, and compared with those of the previously reported **FeCoNi**/C, which clarified the contributory factors of the metal components for the EG electrooxidation activity, C_2 product selectivity, and catalyst durability. The Co-containing catalysts, such as **Co**/C, **FeCo**/C, and **FeCoNi**/C, exhibit relatively high catalytic activities for EG electrooxidation, whereas the catalytic performances of Ni-containing catalysts are relatively low. However, we found that the inclusion of Ni is a requisite for the prevention of rapid degradation due to surface modification of the catalyst. Notably, **FeCoNi**/C shows the highest selectivity for oxalic acid production without CO_2 generation at 0.4 V vs. the reversible hydrogen electrode (RHE), resulting from the synergetic contribution of all of the component elements. Finally, we performed power generation using the direct EG alkaline fuel cell in the presence of the Fe-group catalysts. The power density obtained on each catalyst directly reflected the catalytic performances elucidated in the electrochemical experiments for the corresponding catalyst. The catalytic roles and alloying effects disclosed herein provide information for the design of highly efficient electrocatalysts containing Fe-group metals.

Introduction

The CO_2 concentration in the atmosphere has been inadvertently increased by burning hydrocarbon fuels, leading to serious climate change.[1] Considering the environmental issues related to the CO_2 emission, the development of alternative and sustainable energy circulation systems suppressing the increase of atmospheric CO_2 levels, so called carbon-neutral systems, is regarded as an urgent global tasks.[2] Among energy-carrying materials suitable for widespread use, ethylene glycol ($(CH_2OH)_2$, EG) is an ideal liquid fuel considering its high boiling point (197.3°C) and low vapour pressure (8 Pa at 20°C), which facilitates transportation and storage.[3] Effective EG oxidation catalysts have been widely and intensively sought over the past couple of decades.[4] In recent years, the research has greatly expanded to energy conversion applications through the development of an EG-based fuel cell (FC) employing several electrooxidation catalysts.[5] On another front, the idea of CO_2-free power generation by selective EG oxidation into oxalic acid, $(CO_2H)_2$, which is the second-deepest oxidation product after CO_2 (8-electron oxidation one) has been proposed. Pt-group metals are the main component of anodic electrode catalysts in EG-based FCs (Table S2). However, even the most active Pt catalysts cannot catalyse 8-electron-oxidation but only the 4-electron-oxidation reaction, resulting in the production of glycolic acid. Moreover, fewer examples of EG oxidation catalysts utilizing Fe-group metal elements have been reported.[4b, 6] The development of Fe-group-based catalysts has attracted much attention in view of the replacement of precious elements with abundant elements. Recently, we reported an Fe-group ternary nanoalloy (NA) catalyst supported on carbon, i.e., **FeCoNi**/C, that exhibits catalytic activity for the selective electrooxidation of EG to oxalic acid, resulting in the highly efficient fuel utilization without CO_2 emission.[7] Moreover, power generation using a direct ethylene glycol alkaline fuel cell (DEG-AFC), where **FeCoNi**/C was employed as the anodic electrode catalyst, was also performed. For further cutting-edge applications of Fe-group NA catalysts, a fundamental understanding of the chemical building blocks of the NAs is quite important.

Alloying is a conventional but efficient technique to modulate the chemical properties of pure elements by making use of electronic and geometric interactions among constituent elements[8] that is actively applied as a method to improve catalyst properties. According to the intended use, bimetallic nanoalloy catalysts with an

appropriate structure, such as core-shells,[9] intermetallics,[10] and solid-solutions,[11] have been fabricated and found to show excellent activities and longer catalyst lifetimes than those of monometallic catalysts. Due to synergy effects derived from chemical interactions among constituent elements, a solid-solution type NA can be an efficient catalyst with a wide tuneable range in catalysis. Therefore, an understanding of alloying effects is another crucial issue for the efficient utilization of Fe-group NA catalysts.

In this study, we demonstrate the syntheses of carbon-supported binary NA catalysts, i.e., **FeCo**/C, **FeNi**/C, and **CoNi**/C, and conduct a detailed comparison of their catalytic performances in EG electrooxidation catalysis among a full range of Fe-group catalysts including the ternary NA catalyst, i.e., **FeCoNi**/C, and monometallic nanoparticle (NP) catalysts, i.e., **Fe**/C, **Co**/C, and **Ni**/C, which can provides insight into catalyst design for the selective oxidation of EG to oxalic acid. In addition, *ab initio* calculations for EG oxidation on Fe-group catalysts were carried out, which enables mechanistic understanding of the alloy effects. Moreover, we performed power generation using an alkaline fuel cell fabricated with the prepared Fe-group NAs and NPs as anode catalysts and a solid oxide electrolyte.

Results and Discussions

Syntheses of the carbon-supported Fe-group binary NA catalysts.

Precise control of the metal composition and mixing states of the NA is necessary to guarantee reproducibility and controllability of the catalytic reactions using NA catalysts.[9d, 10b, 11b, 12] To this end, we focused on producing atomically well-mixed Fe-group NA catalysts. A series of carbon-supported Fe-group metal binary NA catalysts, i.e., **FeCo**/C, **FeNi**/C and **CoNi**/C, were prepared using a synthetic methodology for the preparation of **FeCoNi**/C, that we previously reported,[7] including chemical reduction of metal ions and heat-treatment of a mixed-metal-oxide composite under hydrogen atmosphere, in a two-step method.[13] A detailed description of the synthetic procedure is given in the Supplementary Information (SI). As the first step, mixed-oxide precursors were synthesized through the precipitation of small metallic pieces by adding $NaBH_4$ to a triethylene glycol solution containing divalent metal complexes, i.e., $M^{II}(OAc)_2$ (M = Fe, Co, and/or Ni, OAc = $CH_3CO_2^-$) with the co-presence of a carbon support, followed by washing with a mixed solution of acetone and water in air. The desired catalysts were then obtained by treating the precursors under hydrogen at 800°C for 1 minute in the second step. Inductively coupled plasma mass spectroscopy (ICP-MS) results indicate that the metal compositions of the series of NAs were Fe:Co = 45.7:54.3 (for **FeCo**/C), Fe:Ni = 47.3:52.7 (for **FeNi**/C) and Co:Ni = 49.2:50.8 (for **CoNi**/C), with 38.3, 40.1 and 37.0 wt% metal contents, respectively, which reflects the molar ratios in the synthetic step of a precursor (see Table S3).

Bright-field scanning transmission electron microscopy (BF-STEM) images of the prepared catalysts are shown in Fig. 1a, revealing good dispersivity of the NA particles on the carbon support. From these images, the average diameters of the NAs on **FeCo**/C, **FeNi**/C, and **CoNi**/C were determined to be 42±15, 35±15, and 27±7 nm, respectively. The elemental distribution in individual nanoparticles was also examined by assembling energy-dispersive X-ray (EDX) spectroscopy composition maps of Fe, Co, and Ni distributions (shown in blue, red, and green, respectively, in Figs 1b-d). Each element that appears in the overlay of the composition maps shows uniformly mixed-colour particles (Fig. 1e). These results

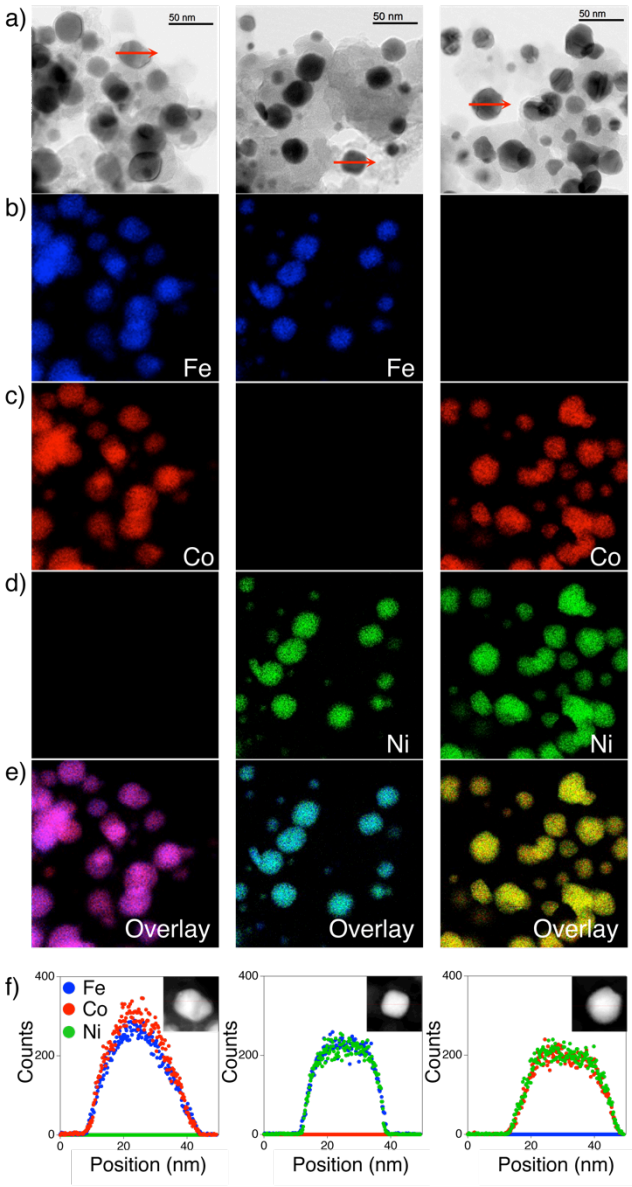

Fig. 1. (a) BF-STEM images and EDX composition maps of the (b) Fe-Kα (blue), (c) Co-Kα (red), (d) Ni-Kα (green) lines, (e) reconstructed overlay maps, and (f) EDX line-scan analysis results of (left) **FeCo**/C, (middle) **FeNi**/C, and (right) **CoNi**/C. Line scans were performed along the arrows marked in (a).

strongly suggest that the constituent elements in each NA are of equal concentration and homogeneous distribution. The uniform distribution is also supported by EDX line-scan analyses. A line profile crossing a single particle is shown in Fig. 1f, where the intensities of characteristic X-rays from the catalysts, Fe-Kα, Co-Kα, and Ni-Kα, are plotted to positions in blue, red, and green, respectively. We can clearly see similar intensity variations for the constituent elements over the whole scanning region. These results are consistent with the ICP-MS results and support the claim that the NAs fabricated on a carbon support are atomically mixed (see also Figs. S1-3). Each powder X-ray diffraction (XRD)[14] pattern of the prepared NA catalyst, shown in Fig. S4, could be attributed to diffraction from a single phase, i.e., NAs on **FeNi**/C and **CoNi**/C have a face-centred cubic (fcc) structure and those on **FeCo**/C have a

body-centred cubic (bcc) structure. These results also suggest that the series of Fe-group NA systems did not form a phase-separated structure but a well-mixed solid solution. Fe-group monometallic NP catalysts, i.e., **Fe**/C, **Co**/C, and **Ni**/C, were also prepared using the synthetic procedures similar to those for the preparation of binary NA catalysts, except for the lower metal loading of **Fe**/C to keep the diameters of the NPs nearly identical. TEM observations revealed that diameters of NPs formed in **Fe**/C, **Co**/C, and **Ni**/C are 28±12, 36±13 and 37±12 nm, respectively (Fig. S5). Chemical and structural characterizations of the NP catalysts were also conducted using ICP-MS and XRD measurements, and the obtained results are summarized in Fig. S6 and Table S4.

Cyclic voltammograms (CVs) and EG electrooxidation activities of the Fe-group binary NA and NP catalysts.

The electrochemical activities of the prepared NA and NP catalysts for EG oxidation were first investigated by cyclic voltammetry (CV). The carbon felt, on which the prepared catalyst was mounted and heat-treated under N_2 and H_2 atmospheres prior to the measurement, was used as the electrode (see SI for details). Fig. 2 shows the CV curves recorded on the binary NA and NP catalysts in basic aqueous solution in a potential range between −1.25 and 1.2 V (vs. a reversible hydrogen electrode (RHE)) together with the curve obtained on **FeCoNi**/C. In the CV measurements on **Fe**/C, **Co**/C, and **FeCo**/C using an alkaline solution without EG, namely, blank measurements, as shown as the black lines in Figs. 2 and S7, current increases approximately 0.2 V (vs. RHE) were commonly observed, which could be assigned to the formation of a metal hydroxide layer ($M + OH^-/M\text{-}OH + e^-$) or self-oxidation of the NAs or NPs.[15] By contrast, in the cases of the **Ni**/C, **CoNi**/C, **FeNi**/C, and **FeCoNi**/C, slight increase in current value approximately 0.2 V (vs. RHE) were obtained. This observation suggests that the surface of Ni-containing catalysts is relatively resistant to chemical modifications of the metal surface in the alkaline solution. When EG was employed in the reaction solution, each catalyst exhibited characteristic behaviour. On the Ni-free catalysts, such as **Fe**/C, **Co**/C, and **FeCo**/C, with the positive-going scan, the current values were reduced compared with those obtained in the blank. It is possible that certain catalyst modifications are caused by the interaction with EG. Moreover, apparent increases in current on **Ni**/C, **FeNi**/C, **CoNi**/C, and **FeCoNi**/C were observed, suggesting that EG oxidation proceeds on these catalysts. Interestingly, among the Ni-containing catalysts, **FeCoNi**/C showed the largest current value. This possibly indicates a relatively high catalytic ability of **FeCoNi**/C for EG oxidation.

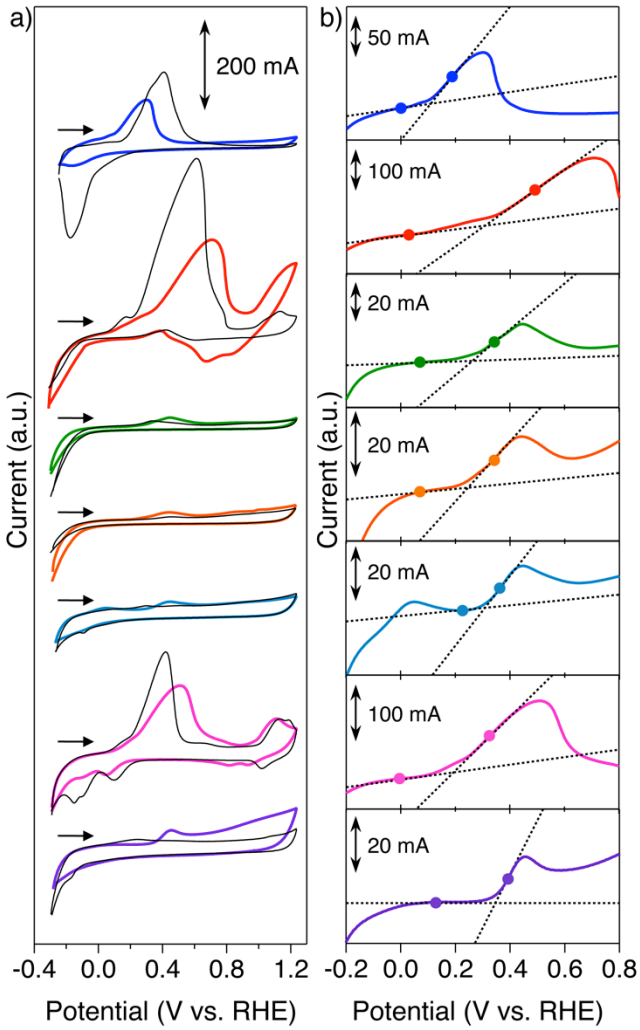

Fig. 2. (a) The cyclic voltammograms using working electrodes coated with **Fe**/C (blue line), **Co**/C (red line), **Ni**/C (green line), **CoNi**/C (orange line), **FeNi**/C (aqua line), **FeCo**/C (pink line), and **FeCoNi**/C (purple line) in 20wt% KOH + 30wt% EG aqueous solution (scan rate: 10 mV/s; Counter electrode: Pt wire; Reference electrode: Hg/HgO in 1 M KOH). Voltammograms recorded in the EG-free 20wt% KOH aqueous solution are shown as black lines. (b) Closed-up curves around the initial rise of current in the positive-going scan with tangential lines before and after the rise (black dashed lines).

EG electrooxidations at a constant potential using chronoamperometry (CA) and oxidized product distributions on the Fe-group NA and NP catalysts.

We then examined the catalytic EG oxidation at a constant potential by using chronoamperometry (CA). To elucidate the catalytic activity and selectivity of the prepared catalysts, quantification of the oxidized products including gaseous products, i.e., CO_2, was investigated. All CA experiments were conducted under anaerobic conditions using a glove box for the prevention of CO_2 contamination from an aerobic atmosphere. Fig. 3 shows the number of electrons generated by each product formation in the EG oxidation, and the current efficiency converted from the number of electrons, corresponding to the product selectivity, at a constant potential of 1.0 V (vs. RHE) applied for 125 min. Detailed definitions for the number of electrons, current efficiency, selectivity, and product distribution are provided in SI[16] and all results are summarized in Figs. S10 and 11. We found that a large quantity of oxidized products was generated on **Co**/C and **FeCo**/C, which correspond to a large number of electrons, as shown in Fig. 3a. These results imply that the large current value observed in the CV measurements on **Co**/C and **FeCo**/C in the EG solution can be attributed to EG oxidation as well as certain catalyst modifications in the alkaline media. Moreover, it should be noted that Co-containing catalysts showed higher catalytic activity not only for EG oxidation but also for the production of C_1 compounds, such as formic acid,

whereas no detectable amount of the oxidized product was obtained on **Fe**/C. These results clearly suggest that the large current wave observed on **Fe**/C in the CV measurement is simply attributable to the catalyst modification in the alkaline medium, and an inclusion of Co enhances the catalytic activity for EG electrooxidation.

Catalytic performances deeply depend on active surface area. In this regard, we should evaluate catalytic activities with consideration for surface areas of NAs and NPs in the catalysts. **Co**/C and **Ni**/C are characterized with similar particle sizes and metal loadings, i.e., 36±13 nm and 48.2wt% for **Co**/C and 37±12 nm and 46.3wt% for **Ni**/C, which means that total surface areas of NPs on the two catalysts are similar. Particle sizes (loadings) of NAs on **FeCo**/C, **FeNi**/C, **CoNi**/C and **FeCoNi**/C are 42±15 (38.3), 35±15 (40.1), 27±7 (37.1) and 25±11 nm (38.1wt%), respectively. Assuming differences in metal loadings on the NA catalysts are negligible, the total surface area of NAs on **FeCo**/C is the smallest. Therefore, high catalytic activities emerging on **Co**/C and **FeCo**/C, which have relatively small surface areas, are attributed to an inherent aspect of Co components.

By contrast, in the case of catalysts containing a relatively larger percentage of Ni, i.e., **Ni**/C, **CoNi**/C, and **FeNi**/C, the number of electrons was considerably smaller than that recorded in the experiments using the other monometallic and binary catalysts. This probably suggests lower catalytic activity of Ni for EG electrooxidation. However, it should be mentioned that these Ni-containing catalysts exhibited low C_1 and high C_2 product selectivities compared with those observed on the Ni-free catalysts. Considering that the C–C bond scission eventually results in CO_2 production, selective EG oxidation to C_2 compounds is an essential requirement to deeply oxidize EG without CO_2 release.[17] Therefore, the inclusion of a certain amount of Ni is important for the selective oxidation to oxalic acid.

Interestingly, the catalysts containing both Fe and Co, such as **FeCo**/C and **FeCoNi**/C, exhibit relatively high selectivity for oxalic acid formation. Combined with the CV and CA results, it is clear that Co-containing catalysts, such as **Co**/C, **FeCo**/C, and **FeCoNi**/C, exhibit high catalytic activities for EG electrooxidation, and the inclusion of Ni improves the durability of the catalysts and enhances the C_2 selectivity. Furthermore, we conclude that the coexistence of Fe and Co promotes the oxalic acid selectivity. Therefore, it is conceivable that **FeCoNi**/C showed the highest selectivity to oxalic acid formation with considerable catalytic efficiency, resulting from the synergistic effect among constituent elements.

To obtain more detailed information about the catalysis, we examined the potential dependence in product distribution on **Co**/C, **FeCo**/C, and **FeCoNi**/C that exhibit relatively high catalytic activities. Fig. 4 shows the current efficiency on these catalysts at 0.4, 0.6, 1.0, and 1.2 V (vs. RHE). With the increase in applied potential, the percentage of the contribution from C_1 compound formation was increased over all of the catalysts. By contrast, at lower potentials, the selectivity for C_2 compound formation was increased. These results suggest that the selectivity in EG electrooxidation can be controlled by the applied potential. At 0.4 V (vs. RHE), a large quantity of C_1 compounds was still produced on **Co**/C and **FeCo**/C, i.e., 12 and 15% in the current efficiency, respectively. On the other hand, on **FeCoNi**/C, C_1 compounds were minimally detected, and the selectivity to oxalic acid was remarkably high, i.e., the selectivity to C_2 compounds and oxalic acid at 0.4 V (vs. RHE) were 99 and 60%, respectively. This result implies that the product distribution more strongly reflects the catalytic nature at a lower applied potential, and the interaction among Fe-group elements can give a favourable environment for selective EG oxidation to oxalic acid. It is also interesting that the current efficiency of **FeCoNi**/C at all potentials, except for 1.2 V (vs. RHE), is higher than that of **Co**/C and **FeCo**/C. These results can be understood in view of the improved tolerance to the alkaline solution upon Ni inclusion.

In the powder XRD patterns of the **Co**/C-employed working electrode after use in the CA measurement held at 1.0 V (vs. RHE) as shown in Fig. S8a, we cannot identify apparent diffraction peaks from Co NPs, which is possibly attributed to the oxidative

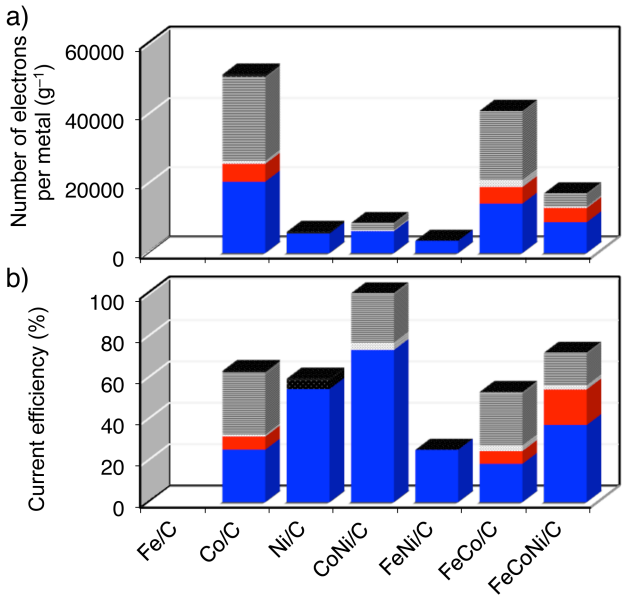

Fig. 3. (a) Number of electrons per metal (gram) in catalysts and (b) current efficiency, related to the oxidized products, glycolic acid (blue), glyoxylic acid (orange), oxalic acid (red), formaldehyde (light grey), formic acid (grey), and CO_2 (black), formations from EG, determined after 125 min of 1.0 V vs. RHE.

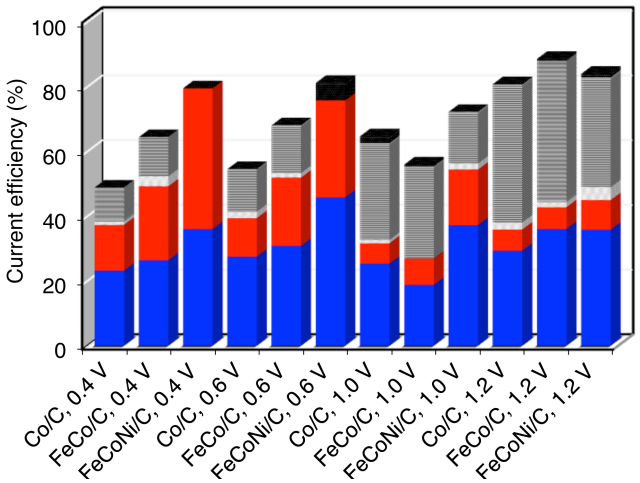

Fig. 4. Current efficiencies, related to the oxidized products, glycolic acid (blue), glyoxylic acid (orange), oxalic acid (red), formaldehyde (light grey), formic acid (grey), and CO_2 (black), formations from EG, determined after 125 min of several constant voltage applications (0.4, 0.6, 1.0 and 1.2 V (vs. RHE) employing **Co**/C, **FeCo**/c, and **FeCoNi**/C catalysts.

dissolution of the metallic parts of the **Co**/C in the reaction. Based on these results, there is a possibility that dissolved Co ions also showed catalytic activity for EG oxidation. By contrast, **FeCoNi**/C once used in the corresponding measurement showed a similar diffraction pattern with that of the starting catalyst (Fig. S8c). This result clearly reflects the higher durability of **FeCoNi**/C catalysts (see Figs. S8, 9). The peak intensity of **FeCoNi**/C was slightly decreased by ~20% after the CA experiment, which might correspond to the ~72% current efficiency of **FeCoNi**/C in CA at 1.0 V (vs. RHE).

Theoretical calculation of C-C bond dissociation activation energy in EG oxidation processes on Fe-group metal surface.

To clarify the reason why oxalic acid and C_2 compounds (especially oxalic acid) are selectively generated on **FeCoNi**/C, we calculated activation energies for the C-C bond dissociation of glycolic acid on **FeCo** and **FeCoNi** NA surfaces by a first-principles method. The glycolic acid ($HOCH_2$-CO_2H) is generated by the 4-electron oxidation of EG, and gives oxalic acid by further 4-electron oxidation. Therefore, it is probable that glycolic acid is generated at the first stage of the EG oxidation forming oxalic acid on prepared catalysts. Considering the crystal structures of the NAs, i.e., **FeCoNi** and **FeCo** NAs having fcc and bcc structures, the periodically repeated slabs of the three atomic layers were used for the **FeCo**(001) and **FeCoNi**(111) surface models. To construct the realistic surface models, Fe, Co, and Ni atoms were uniformly arranged in the alloys based on our experimental results indicating that alloy components are well mixed in FeCoNi/C and FeCo/C (see Ref. 7 and Fig. S1). Detailed calculation methods are described in SI. We first determined the initial structures of the glycolic acid molecule on the alloy surfaces. Table S5 represents the adsorption energy of glycolic acid with various configurations on **FeCo**(001) and **FeCoNi**(111) and Figs. S12a and c show the most stable structures of glycolic acid on **FeCo**(001) and **FeCoNi**(111), respectively. Our calculation proved that, at the initial stages, the oxygen atoms of glycolic acid are located above the Fe atoms on both surfaces. This indicates the bonding interaction between the oxygen atoms of a glycolic acid molecule and Fe atoms on the catalyst surface during the initial stage of the reaction. Figs. S12b and d denote the molecular configuration after C-C bond dissociation on **FeCo**(001) and **FeCoNi**(111), respectively. The calculated energy diagram for the C-C bond dissociation of glycolic acid on the **FeCo**(001) and **FeCoNi**(111) are described in Fig. 5.

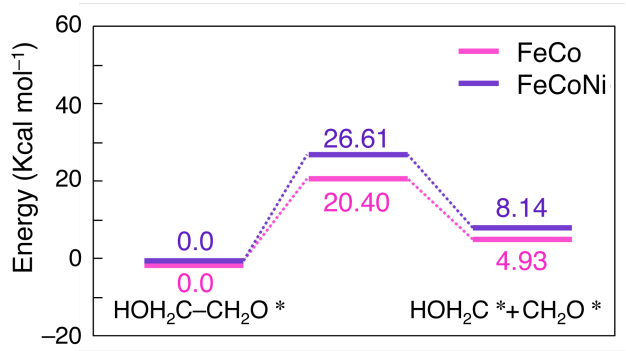

Fig. 5. Energy diagrams for the C-C bond scission of glycolic acid on **FeCo**(001) and **FeCoNi**(111). An origin of energy is set to the energy in the initial state of each reaction path.

This diagram presents that the activation energies for the C-C bond dissociation on the **FeCo**(001) and **FeCoNi**(111) are 20.40 and 26.61 kcal/mol, respectively. This energetic difference matches the observed experimental result that **FeCo** catalyst more easily generates C_1 compounds, plausibly by the C-C bond breaking reaction of glycolic acid and/or EG.

Next, we listed the charges and C-C bond distances of the glycolic acid adsorbed on **FeCo**(001) and **FeCoNi**(111) at the initial, transition, and final states in the C-C bond dissociation process (Table S6). The C-C bond lengths at the transition state on the **FeCo**(001) and **FeCoNi**(111) surfaces are 2.745 and 2.488 Å, respectively. The large difference in the estimated C-C bond between **FeCo**(001) and **FeCoNi**(111) at the transition state could be attributed to the difference in the activation energies for the C-C bond dissociation in these alloys. In brief, the C-C bond of glycolic acid is more easily dissociated on **FeCo**(001) than on **FeCoNi**(111).

Chemical bond dissociation could be initiated by the electron transfer between the adsorbed glycolic acid molecule and the metal surface. Then, we focused on the charge value of the glycolic acid molecule at each state. The charge values of the glycolic acid at the initial and transition states on **FeCo**(001) were found to be -0.468 and -0.346, respectively, whereas those on **FeCoNi**(111) were -0.391 and -0.342 (Table S5). The estimated differences in the charge value on the glycolic acid between the initial and transition states on **FeCo**(001) and **FeCoNi**(111) were determined to be 0.122 and 0.049, respectively. For clarification of the reason for the difference in the number of electrons transferred from the alloy surfaces to substrates, we described the density of states (DOS) of *d* orbitals and the *d*-band centers on both surface models in Fig. S13. The energy level of the lowest unoccupied molecular orbital (LUMO) of glycolic acid is also provided. In Fig. S13, the origin of energy corresponds to a vacuum level. The energy level of LUMO of glycolic acid is -54.98 kcal/mol. The *d*-band center on **FeCo**(001) and **FeCoNi**(111) is -142.55 kcal/mol and -169.17 kcal/mol, respectively. Fig. S13 shows the larger difference of the energy levels between the LUMO and the *d*-band center on FeCoNi(111), which leads to the smaller degree of charge transfer between glycolic acid and **FeCoNi**(111). The smaller charge difference on **FeCoNi**(111) is associated with the shorter C-C length on the **FeCoNi** alloy. Therefore, we can consider that the higher activation energy for the C-C bond dissociation on the **FeCoNi**(111) surface is attributable to the smaller charge transfer from the alloy surface to the substrate molecule, which accounts for the high C_2 and oxalic acid selectivity observed on **FeCoNi**/C.

Power generation on Fe-group NA and NP catalysts using a direct EG alkaline fuel cell.

We examined the performance of DEG-AFCs employing NA catalysts that exhibit relatively high catalytic activities in CV and CA experiments, i.e., **FeCo**/C and **FeCoNi**/C and monometallic NP catalysts. The potentiodynamic and power density curves obtained with 10wt% EG in a 10wt% KOH aqueous solution at 70 °C using the previously reported AFC set[17a] employing the Fe-group catalysts as an anode electrocatalyst are shown in Fig. 6, and parameters, i.e., open circuit voltages and peak power densities are summarized in Table S7. In comparing the monometallic catalysts employing AFCs, the order of power output is **Fe**/C < **Ni**/C < **Co**/C, which matches with the catalytic performance discussed above in the electrochemistry section, suggesting the remarkable influence in

AFC output from applied anodic electrode catalysts and the potential effectiveness of these Fe-group metal catalysts as a part of power generation devices. Although, other factors, that affect to AFC power output should also be taken into account, NA catalysts employing AFCs, i.e., **FeCo**/C and **FeCoNi**/C, generally showed higher AFC performances than those of monometallic catalysts employing AFCs. Considering the C_2 and oxalic acid selectivities determined in CA experiments, **FeCoNi**/C satisfies the need for efficient power generation with no CO_2 emission.

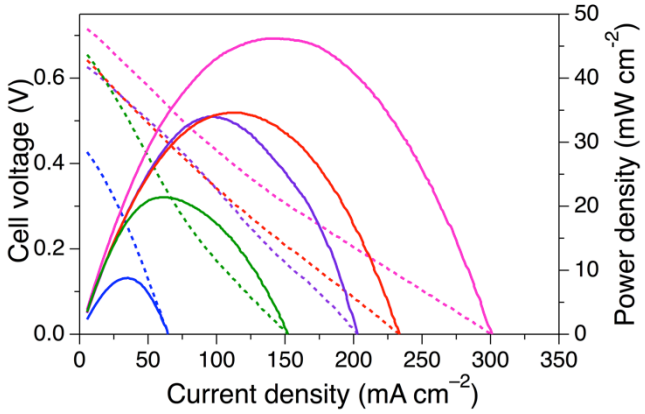

Fig. 6. Polarization and power density curves measured in DEG-AFCs containing **Fe**/C (blue lines), **Co**/C (red lines), **Ni**/C (green lines), **FeCo**/C (pink lines), and **FeCoNi**/C (purple lines) electrocatalysts. Cell voltage and power density are shown in dotted and solid lines, respectively.

Conclusions

We prepared a series of Fe-group binary and monometal catalysts and investigated their structural and catalytic properties for EG electrooxidation in alkaline media. Electrochemical experiments, using CV and CA methods revealed the roles of each Fe-group metal. Co-containing catalysts, such as **Co**/C and **FeCo**/C, showed considerably high activity, reflecting the characteristics of Co as a reaction centre for the EG electrooxidation. The inclusion of Ni was found to improve the catalyst durability. Fe-containing NA catalysts, such as **FeCo**/C and **FeCoNi**/C, exhibited relatively high selectivity to oxalic acid. As a result of the synergistic effects among the constituent elements, the ternary NA catalyst, i.e., **FeCoNi**/C, served as a highly selective catalyst for oxalic acid production in the EG electrooxidation. Furthermore, the performances of the DEG-AFC directly reflect the catalytic characters of the Fe-group metals as observed in the electrochemical experiments. These findings are the first systematic results on the catalytic natures of Fe-group electrocatalysts, which have been previously regarded as inactive anode materials. Although further improvements in the activity of purely Fe-group catalysts are needed for their practical use, elucidation of the catalytic roles of Fe-group metals will contribute to performance enhancement and sustainable procurement of electrocatalysts by the rational design of active catalysts including Fe-group metals.

Experimental Section

General Procedures.

All synthetic operations and measurements in this study were performed under a N_2 atmosphere. The gases used in this study were supplied by Fukuoka Oxygen Mfg Co. Ltd. and had the following purities: N_2, 99.99%; H_2, 99.99%; He, 99.99%; Ar, 99.99%; 5%H_2/95%Ar, 99.99%. All reagents were used as received.

Preparation of Fe-group Binary NA (FeCo/C, FeNi/C, and CoNi/C) and Monometallic NP (Co/C and Ni/C) Catalysts.

Fe-group NA and monometallic NP catalysts were prepared using a similar procedure to that described below, except for the scale of starting materials, reagents, and solvents used, which are summarized in Table S1. $Fe^{II}(OAc)_2$ (*A* mg, *B* mmol, Tokyo Kasei Kogyo), $Co^{II}(OAc)_2{\cdot}4H_2O$ (*C* mg, *D* mmol, Wako), and $Ni^{II}(OAc)_2{\cdot}4H_2O$ (*E* g, *F* mmol, Wako) were dissolved in a mixed solvent consisting of polyethylene glycol (PEG, M_W = approx. 1,500, *G* g, Wako) and triethylene glycol (TEG, *H* mL, Kishida). After vigorous stirring with bubbling Ar for 30 min at room temperature, the reaction mixture was heated to 80°C and kept stirred for 30 min. The MeOH (*I* mL) suspension of carbon black (Vulcan, XC-72R, *J* g, Cabot Corporation) was added to this dark-brown solution, and stirred for 30 min at room temperature. After stirring at 80°C for 3 min, an aqueous solution (*K* mL) of $NaBH_4$ (*L* g, Wako) was added to the mixture. The resultant mixture was stirred at 80°C for 3 min, and then cooled to room temperature. After the addition of acetone (*M* mL) and Et_2O (*N* mL), a black precipitate was obtained and separated from the supernatant solution by centrifugation and decantation. The precipitate was washed three times with a mixed solution of water and acetone, and the catalyst precursor was obtained by drying the precipitate in vacuo. The carbon-supported NA catalyst was prepared by the thermochemical processing of the precursor, the details of which were previously reported.[10b-d, 11b, 18] The precursor including the oxide composites was treated at 800°C under 5%H_2/95%Ar for 1 min to provide a carbon-supported alloy catalyst (*O* g). ICP-MS measurement was made using an Agilent 7500c (Agilent Technologies, Inc.), and the results are tabulated in Table S2.

We found that Fe NPs supported on carbon with metal loading higher than 40 wt% tend to have diameters of more than approx. 90 nm. To eliminate the need to consider size effects on catalytic activity, **Fe** NPs supported on carbon having an average diameter similar to that of the Fe-group binary NA (**FeCo**/C, **FeNi**/C, and **CoNi**/C) and monometallic NP (**Co**/C and **Ni**/C) were prepared by adjusting the metal loading. $Fe^{II}(OAc)_2$ (0.1396 g, 0.8 mmol) was dissolved in a mixed solvent of PEG (0.3525 g) and TEG (200 mL). After vigorous stirring with bubbling Ar for 30 min at room temperature, the reaction mixture was heated to 80°C and kept stirred for 30 min. The MeOH (10 mL) suspension of Vulcan (0.083 g) was added to this pale-brown solution, and stirred for 30 min at room temperature. After stirring at 80°C for 3 min, an aqueous solution (10 mL) of $NaBH_4$ (0.3029 g) was added. The metal-oxide composite and carbon-supported Fe monometallic NP catalysts were prepared in a similar manner to that of the Fe-group binary NAs (**FeCo**/C, **FeNi**/C, and **CoNi**/C) and monometallic NPs (**Co**/C and **Ni**/C). The results of ICP-MS are tabulated in Table S3.

BF-STEM, HAADF-STEM, EDX, and Line-scan Analyses.

Bright field scanning transmission electron microscopy (BF-STEM), high-angle annular dark field scanning transmission electron microscopy (HAADF-STEM) images, energy dispersive X-ray spectroscopy (EDX) analyses, and line scan analyses of Fe-group binary NA catalysts (**FeCo**/C, **FeNi**/C, and **CoNi**/C) were recorded with a JEM-ARM200F operated at 120 kV to identify the shape and dispersion of the particles and to analyse the distribution of Fe, Co, and Ni atoms in the particle interior. For these measurements, catalysts were suspended in methanol solution and ultrasonicated using a pulse ultrasonic probe for 20 min. The suspension was dropped onto the carbon-coated copper grid followed by solvent evaporation in vacuo at room temperature overnight (approximately 12 hours). The measuring interval was 0.2 nm for all measurements in the STEM analyses.

Notes and references

† Electronic Supplementary Information (ESI) available: General procedures, synthetic operations, measurement (powder XRD, cyclic voltammetry, and chronoamperometry) and definition of number of electrons, current efficiency, selectivity, chemical composition of NA and NP catalysts, EDX line scan analyses results, TEM images of NP catalysts, CV curves of Fe-group NA catalysts, adsorption configuration of glycolic acid on FeCo(001) and FeCoNi(111) surfaces, and change of the C-C bond distances of glycolic acid on their surface. See DOI: 10.1039/c000000x/

[a] International Institute for Carbon Neutral Energy Research (WPI-I^{2}CNER), Kyushu University, Motooka 744, Nishi-ku, Fukuoka 819-0395, Japan.
[b] CREST, JST, 4-1-8 Honcho, Kawaguchi, Saitama 332-0012, Japan.
[c] Department of Applied Quantum Physics and Nuclear Engineering, Kyushu University, Motooka 744, Nishi-ku, Fukuoka 819-0395, Japan.
[d] RIKEN SPring-8 Center, 1-1-1 Kouto, Sayo-cho, Sayo-gun, Hyogo 679-5148, Japan.
[e] Department of Chemistry and Bioengineering, Faculty of Engineering, Iwate University, 4-3-5 Ueda, Morioka, Iwate 020-8551, Japan.
[f] Fracture and Reliability Research Institute (FRRI), Graduate School of Engineering, Tohoku University, 6-6-11 Aoba, Aramaki, Aoba-ku, Sendai 980-8579, Japan.

1. P. M. Cox, R. A. Betts, C. D. Jones, S. A. Spall and I. J. Totterdell, *Nature*, 2000, **408**, 184-187.
2. (a) N. Armaroli and V. Balzani, *Angew. Chem. Int. Ed.*, 2007, **46**, 52-66; (b) S. Chu and A. Majumdar, *Nature*, 2012, **488**, 294-303; (c) R. Watanabe, M. Yamauchi, M. Sadakiyo, R. Abe and T. Takeguchi, *Energy Environ. Sci*., 2015, in press, DOI; 10.1039/C5EE00192G.
3. *U.S. Environmental Protection Agency. Health Effects Assessment for Ethylene Glycol. EPA/600/8-88/038. Environmental Criteria and Assessment Office, Office of Health and Environmental Assessment, Office of Research and Development, Cincinnati, OH. **1988**.*
4. (a) Y. Kwon, S. C. S. Lai, P. Rodriguez and M. T. M. Koper, *J. Am. Chem. Soc.*, 2011, **133**, 6914-6917; (b) S. C. Chang, Y. Ho and M. J. Weaver, *J. Am. Chem. Soc.*, 1991, **113**, 9506-9513; (c) A. Kumar, *J. Am. Chem. Soc.*, 1981, **103**, 5179-5182; (d) S. Yongprapat, A. Therdthianwong and S. Therdthianwong, *J. Electroanal. Chem.*, 2013, **697**, 46-52; (e) J.-L. Lin, J. Ren, N. Tian, Z.-Y. Zhou and S.-G. Sun, *J. Electroanal. Chem.*, 2013, **688**, 165-171; (f) F. Kosaka, Y. Oshima and J. Otomo, *Electrochim. Acta*, 2011, **56**, 10093-10100; (g) K. Miyazaki, T. Matsumiya, T. Abe, H. Kurata, T. Fukutsuka, K. Kojima and Z. Ogumi, *Electrochim. Acta*, 2011, **56**, 7610-7614; (h) T. Ramulifho, K. I. Ozoemena, R. M. Modibedi, C. J. Jafta and M. K. Mathe, *J. Electroanal. Chem.*, 2013, **692**, 26-30; (i) H. Yue, Y. Zhao, X. Ma and J. Gong, *Chem. Soc. Rev.*, 2012, **41**, 4218-4244.
5. (a) V. Livshits, M. Philosoph and E. Peled, *J. Power Sources*, 2008, **178**, 687-691; (b) A. Serov and C. Kwak, *Appl. Catal. B: Environ.*, 2010, **97**, 1-12; (c) L. Xin, Z. Zhang, J. Qi, D. Chadderdon and W. Li, *Appl. Catal. B: Environ.*, 2012, **125**, 85-94; (d) A. Marchionni, M. Bevilacqua, C. Bianchini, Y.-X. Chen, J. Filippi, P. Fornasiero, A. Lavacchi, H. Miller, L. Wang and F. Vizza, *ChemSusChem*, 2013, **6**, 518-528; (e) V. Bambagioni, M. Bevilacqua, C. Bianchini, J. Filippi, A. Marchionni, F. Vizza, L. Q. Wang and P. K. Shen, *Fuel Cells*, 2010, **10**, 582-590.
6. (a) V. L. Oliveira, C. Morais, K. Servat, T. W. Napporn, G. Tremiliosi-Filho and K. B. Kokoh, *Electrochim. Acta*, 2014, **117**, 255-262; (b) B. Wieland, J. P. Lancaster, C. S. Hoaglund, P. Holota and W. J. Tornquist, *Langmuir*, 1996, **12**, 2594.
7. T. Matsumoto, M. Sadakiyo, M. L. Ooi, S. Kitano, T. Yamamoto, S. Matsumura, K. Kato, T. Takeguchi and M. Yamauchi, *Sci. Rep.*, 2014, **4**, 5620.
8. R. Ferrando, J. Jellinek and R. L. Johnston, *Chem. Rev.*, 2008, **108**, 845-910.
9. (a) S. Koh and P. Strasser, *J. Am. Chem. Soc.*, 2007, **129**, 12624-12625; (b) J. X. Wang, H. Inada, L. Wu, Y. Zhu, Y. Choi, P. Liu, W.-P. Zhou and R. R. Adzic, *J. Am. Chem. Soc.*, 2009, **131**, 17298-17302; (c) A. U. Nilekar, S. Alayoglu, B. Eichhorn and M. Mavrikakis, *J. Am. Chem. Soc.*, 2010, **132**, 7418-7428; (d) S. Alayoglu, A. U. Nilekar, M. Mavrikakis and B. Eichhorn, *Nat. Mater.*, 2008, **7**, 333-338.
10. (a) A. Miura, H. Wang, B. M. Leonard, H. c. D. Abruña and F. J. DiSalvo, *Chem. Mater.*, 2009, **21**, 2661-2667; (b) M. Nakaya, M. Kanehara, M. Yamauchi, H. Kitagawa and T. Teranishi, *J. Phys. Chem. C*, 2007, **111**, 7231-7234; (c) M. Yamauchi and T. Tsukuda, *Dalton Trans.*, 2011, **40**, 4842-4845; (d) M. Okada, A. Kamegawa, J. Nakahigashi, A. Yamaguchi, A. Fujita and M. Yamauchi, *Mater. Sci. Eng., B*, 2010, **173**, 253-259.
11. (a) K. Kusada, H. Kobayashi, R. Ikeda, Y. Kubota, M. Takata, S. Toh, T. Yamamoto, S. Matsumura, N. Sumi, K. Sato, K. Nagaoka and H. Kitagawa, *J. Am. Chem. Soc.*, 2014; (b) M. Yamauchi, R. Abe, T. Tsukuda, K. Kato and M. Takata, *J. Am. Chem. Soc.*, 2011, **133**, 1150-1152; (c) Y. Shiraishi, H. Sakamoto, Y. Sugano, S. Ichikawa and T. Hirai, *ACS Nano*, 2013, **7**, 9287-9297.
12. (a) B. Coq and F. Figueras, *J. Mol. Catal. A: Chem.*, 2001, **173**, 117-134; (b) Y. Ohkubo, M. Shibata, S. Kageyama, S. Seino, T. Nakagawa, J. Kugai, H. Nitani and T. Yamamoto, *J. Mater. Sci.*, 2013, **48**, 2142-2150.
13. M. J. Sharif, M. Yamauchi, S. Toh, S. Matsumura, S.-i. Noro, K. Kato, M. Takata and T. Tsukuda, *Nanoscale*, 2013, **5**, 1489-1493.
14. K. Kato, R. Hirose, M. Takemoto, S. Ha, J. Kim, M. Higuchi, R. Matsuda, S. Kitagawa and M. Takata, *AIP Conf. Proc.*, 2010, **1234**, 875-878.
15. (a) N. R. Elezovic, B. M. Babic, L. M. Vracar, V. R. Radmilovic and N. V. Krstajic, *PCCP*, 2009, **11**, 5192-5197; (b) J. L. Cohen, D. J. Volpe and H. D. Abruna, *PCCP*, 2007, **9**, 49-77; (c) H. Wang, L. R. Alden, F. J. DiSalvo and H. c. D. Abruña, *Langmuir*, 2009, **25**, 7725-7735.
16. (a) T. Matsumoto, M. Sadakiyo, M. L. Ooi, T. Yamamoto, S. Matsumura, K. Kato, T. Takeguchi and M. Yamauchi, *submitted*; (b) A. J. Bard and L. R. Faulkner, *Electrochemical Methods: Fundamentals and Applications*, John Wiley & Sons, Inc.: New York, 2001.
17. (a) T. Takeguchi, H. Arikawa, M. Yamauchi and R. Abe, *ECS Trans.*, 2011, **41**, 1755-1759; (b) S. P. Annen, V. Bambagioni, M. Bevilacqua, J. Filippi, A. Marchionni, W. Oberhauser, H. Schönberg, F. Vizza, C. Bianchini and H. Grützmacher, *Angew. Chem. Int. Ed.*, 2010, **49**, 7229-7233; (c) C. Bianchini and P. K. Shen, *Chem. Rev.*, 2009, **109**, 4183-4206; (d) V. Bambagioni, C. Bianchini, A. Marchionni, J. Filippi, F. Vizza, J. Teddy, P. Serp and M. Zhiani, *J. Power Sources*, 2009, **190**, 241-251; (e) K. Matsuoka, Y. Iriyama, T. Abe, M. Matsuoka and Z. Ogumi, *J.*

Power Sources, 2005, **150**, 27-31; (f) J. A. Cracknell, K. A. Vincent and F. A. Armstrong, *Chem. Rev.*, 2008, **108**, 2439-2461; (g) C. Bianchini, V. Bambagioni, J. Filippi, A. Marchionni, F. Vizza, P. Bert and A. Tampucci, *Electrochem. Commun.*, 2009, **11**, 1077-1080.

18. H. Kobayashi, M. Yamauchi, R. Ikeda and H. Kitagawa, *Chem. Commun.*, 2009, 4806-4808.